Available online at www.sciencedirect.com
SCIENCE DIRECT®
Cement & Concrete Composites 28 (2006) 77–89
Cement & Concrete Composites
www.elsevier.com/locate/cemconcomp

Analytical simulation of tensile response of fabric reinforced cement based composites

Barzin Mobasher [a,*], Jitendra Pahilajani [a], Alva Peled [b]

[a] Department of Civil and Environmental Engineering, Arizona State University, P.O. Box 875306, Tempe, AZ 85287-5306, USA
[b] Department of Structural Engineering, Ben Gurion University, Beer Sheva, Israel

Received 27 December 2004; received in revised form 16 March 2005; accepted 2 June 2005
Available online 12 September 2005

Abstract

A model simulating the tensile behavior of fabric–cement composites is presented to relate the properties of the matrix, fabric, interface and the damage parameters to the overall mechanical response of the composites. Crack spacing parameters measured during tensile tests are used to define the damage parameters, and related to the stiffness degradation as a function of the applied strain. This procedure is integrated in composite laminate theory using an incremental approach to model the uniaxial tensile response. Two approaches of linear and nonlinear fabric bridging models are used. The model is capable of using interface parameters for different fabrics, matrix properties, and processing parameters. Simulation results are studied by means of parametric simulation and a validation of a variety of experimental observations which vary the matrix formulation with flyash, changes in pressure after casting, and fabric type.

Keywords: Fabric reinforced composites; Cement composites; Laminated composites; Pultrusion; Fibers; Fabrics; Toughness; Strength; Microcracking; Toughening; Damage mechanics; Stress–strain; Alkali resistant glass fibers; Polypropylene fabrics

1. Introduction

Fabric reinforced cement composites constitute a recent addition to the family of cement based composite materials [1,2]. Various research groups have developed a wealth of recent information pertaining the methodologies, properties, and areas of applications for fabric reinforced cement based materials [3–5]. Very encouraging tensile strength and ductility responses have been observed by various experimental programs with tensile strength of the order of 20–25 MPa and tensile strain capacity of 3–5% [6,7]. Theoretical modeling of the toughening mechanisms is still lacking. The tensile behavior of fabric–cement composites is simulated using a model that relates the properties of the matrix, fabric, interface, and the damage parameters. The formulation can be easily extended to various matrix and fabric systems under biaxial, flexural, and shear type loading conditions. Parameters of interest include of the effects of fabric material, matrix, and the processing conditions on the strength, ductility, and strain capacity.

The proposed method is based on the ply discount method of classical laminate theory [8], where the fabrics and matrix are modeled as discrete phases. An incremental approach which updates the stiffness of the nonlinear matrix phase at each loading increment is used and various aspects of stress–strain relationship, stiffness degradation, and distributed crack formation are combined. A model which relates the crack spacing evolution and stiffness degradation of the composite to the applied strain is introduced. An anisotropic scalar damage parameter is also used to relate the axial strain to the

* Corresponding author. Fax: +1 480 965 0141.
E-mail address: barzin@asu.edu (B. Mobasher).

0958-9465/$ - see front matter © 2005 Elsevier Ltd. All rights reserved.
doi:10.1016/j.cemconcomp.2005.06.007

reduction in crack spacing [9,10], while other critical parameters include the stiffness of the cement–fabric system during debonding and pullout.

The geometric pattern of fabric consisting of a large number of interconnected longitudinal and transverse fill yarns, develops an excellent bond with cement matrix by mechanical interlock and anchorage of yarns [11]. This enhancement must be evaluated in the context of bond stiffness, which maintains the newly formed cracks at a minimal width while transferring the loads back into matrix. High bond stiffness and strength promotes matrix cracking as opposed to fabric debonding and pullout, resulting in strong and ductile composites with dense crack pattern. The pullout–slip behavior of the fabric during loading serves to act as an important parameter in bridging the matrix cracks. Distributed cracking takes place due to the high stiffness of the fabric pullout response, which results in rapid transfer of the load back into the matrix.

Two types of fabric bridging across a matrix crack system are used to relate the interface bond properties to the strengthening and toughening of fabric–cement composites. In the linear approach the experimentally obtained fabric interface stiffness parameters are used as linear spring elements to bridge the matrix cracks. In the nonlinear approach, the first step of simulation deals with formulation of the theoretical fabric pullout response as affected by the parameters of interface and calibration of experimental pullout results to measure the interfacial properties. The variables are the embedded length, fabric sizing, yarn distribution (volume fraction), strength of the junctions within a fabric and the stiffness of the matrix, fabric, longitudinal and transverse interfaces. A model to generate pullout–slip response of fabric has been developed recently [12] and briefly addressed in Appendix I. Using this simulated pullout–slip response model in the tension response the load–displacement relationship for the composite is obtained. Model simulation data is compared with the wide range of experimental tests to explain the effects of various materials and processing parameters on the mechanical response of cement based fabric reinforced composites.

2. Experimental observations of nonlinear stress–strain response

A comprehensive experimental program was conducted to study the effect of fabric type, matrix formulations, and processing parameters on the mechanical response of cement based composites [6]. Using closed loop tensile tests stress–strain response as well as automated procedures to measure spacing between the cracks formed during testing were used. Details of the experimental program and fabric parameters are presented in additional references by Peled and Mobasher [7,13]. Selected experimental results are used in this work to address the modeling challenges for fabric–cement systems.

Table 1 summarizes the mix properties and processing method for the various composites used in the theoretical simulation while Table 2 shows the geometry of the fabrics. In both woven and bonded fabrics, two sets of perpendicular yarns are connected together to form a fabric structure. In the woven fabric the yarns are connected by friction when one set of yarns pass above and under the other set, where in the bonded fabric the two sets are connected together by a polymeric adhesive. In the knitted fabric the two transverse yarns in the x and y directions are sewn by a third yarn which is in the z direction. Parameters listed in Tables 1 and 2 are referred as systems A–E. They are used to address the effects of: (a) fabric type and geometry (high modulus bonded AR-Glass, low modulus woven polyethylene (PE), and low modulus knitted polypropylene (PP)),

Table 1
Summary of mix properties and processing method for the various composites used

Mix	Cement (g)	Flyash (g)	Silicafume (g)	w/cm	Fabric material	Processing	Pressure (kPa)
A	7681	0	1346	0.4	AR-Glass	Pultrusion	1.7
B	5948	3836	822	0.4	AR-Glass	Pultrusion	1.7
C	7681	0	1346	0.4	AR-Glass	Pultrusion	15.0
D	7681	0	1346	0.4	PE	Pultrusion	15.0
E	7681	0	1346	0.4	PP	Pultrusion	15.0

Table 2
Geometry of fabrics

Fabric material	Fabric type	Yarn type	Height of fill yarn (mm)	Thickness of fill yarn (mm)	Distance between yarns (mm)	Number of fill yarn per 1 mm
AR-Glass	Bonded	Bundle	1.778	0.356	3.810	0.2
PE	Woven	Monofilament	0.254	0.356	0.254	0.6
PP	Knitted	Bundle	0.381	0.254	0.381	0.3

(b) matrix formulations (with and without addition of fly ash), and (c) processing parameters (low and high normal pressures applied to the composite after casting).

Fig. 1 represents a typical tensile stress–strain response of AR-Glass fabric reinforced cement composite represented as Series A in Tables 1 and 3. The tensile response shows a linear behavior up to about 3 MPa, beyond this level the stress–strain response becomes nonlinear, while a major change in the stiffness of the sample occurs at bend over point (BOP) around 3–4 MPa. The BOP is characterized by a knee in the stress–strain curve and identified by its lower and upper bound estimates (BOP^-, and BOP^+). The specimen continues to carry load at a significantly lower stiffness up to an ultimate strain level of 6%. In the region between the BOP and ultimate strength, cracking is differentiated as formation of distributed cracks, and later on as widening of existing cracks. The material property data corresponding to these stages are presented for various fabric cement based systems in Table 3. All these specimens were tested after 7 days of curing. The experimental data consist of a range of parameters in terms of the initial stiffness, BOP stress (lower and upper bound levels indicated by − and + signs), BOP strain, post BOP stiffness, ultimate strength capacity, toughness [14] and pullout stiffness.

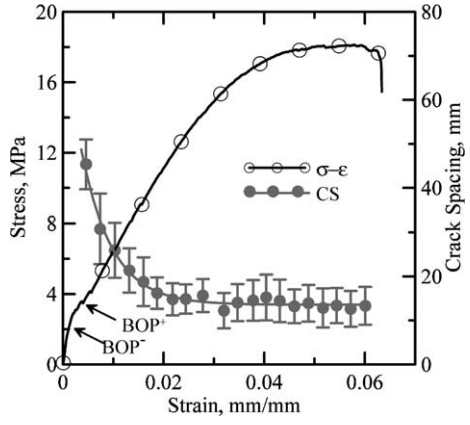

Fig. 1. The crack spacing and stress as a function of applied strain for the AR-Glass fabric reinforced cement based composite (Series A).

3. Distributed cracking and spacing evolution

In order to quantitatively measure the crack spacing and its distribution, an automated procedure based on image analysis was developed by Mobasher, et al. [9,13]. This approach results in a statistically viable sampled set of data collected at each strain level. An empirically based damage evolution law was obtained from the experimental results of average crack spacing as a function of applied strain. An exponentially decaying function representing the crack spacing versus stain is given by

$$S(\varepsilon_i) = S_1 + S_0 e^{-\alpha(\varepsilon_i - \varepsilon_{mu})} \qquad \varepsilon_i > \varepsilon_{mu} \tag{1}$$

where S is average crack spacing; S_1 is a parameter describing saturation crack spacing; S_0 and α are parameters describing the decay rate; ε_i is strain at which the spacing is computed; ε_{mu} is strain at the BOP(+) level. The function representing crack spacing is also plotted in Fig. 1 and indicates an inverse relationship with applied strain. At sufficiently high strain levels a saturation level is reached as indicated by the flattening of the crack spacing curve at about 12 mm. Beyond this point, reduction in crack spacing is not observed, as further increase in the strain causes widening of existing cracks by fabric pullout. Typical values of S_1, S_0, ε_{mu} and α for different matrix and fabric combinations are given in Table 4. In addition, parameters X_1, X_2 and X_3 for the function representing reduction in stiffness, which has a similar form as Eq. (1), are also provided in the same table. The numbers represent an average value of three replicate specimens.

Table 3
Experimental values of mechanical properties of composite systems used in the theoretical simulation [14,15,23]

Mix	Designation	Values	E_i (MPa)	$\sigma_{BOP(-)}$ (MPa)	$\sigma_{BOP(+)}$ (MPa)	$\varepsilon_{BOP(-)}$ (%)	$\varepsilon_{BOP(+)}$ (%)	E_p (MPa)	σ_{ult} (MPa)	ε_{ulti} (%)	Toughness (MPa)	Pullout stiffness (N/mm)
A	ARGNP	Avg	2085	1.26	3.36	0.069	0.232	363	14.28	4.637	0.44	244.47
		(Std)	(297)	(0.61)	(1.42)	(0.039)	(0.143)	(103)	(2.61)	(0.717)	(0.04)	(57.9)
B	ARG-FA	Avg	2910	1.40	5.42	0.047	0.469	511	18.7	4.7	0.78	216.72
		(Std)	(1137)	(0.71)	(0.47)	(0.017)	(0.167)	(150)	(8.25)	(1.81)	(0.39)	(41.5)
C	ARG-P900	Avg	3732	2.73	5.15	0.095	0.234	639	16.29	2.43	0.26	216.72
		(Std)	(479)	(1.23)	(1.42)	(0.046)	(0.045)	(148)	(5.81)	(0.387)	(0.12)	(41.5)
D	PE-P900	Avg	2436	1.70	4.35	0.085	0.174	81	7.21	3.73	0.21	7.06
		(Std)	(411)	(0.60)	(0.32)	(0.049)	(0.026)	(14)	(0.70)	(0.035)	(0.02)	(1.1)
E	PP-P900	Avg	1698	1.96	5.30	0.073	0.128	354	10.18	5.23	0.51	109.04
		(Std)	(817)	(1.02)	(0.22)	(0.000)	(0.003)	(6)	(1.77)	(0.034)	(0.03)	(13.4)

E_i = Initial stiffness.
E_p = Post-crack stiffness.
BOP = Bend over point ('−' refers to the lower bound estimate and '+' refers to the upper bound estimate of stress). Pullout stiffness was measured as the slope of force versus slip during the pullout test of fabrics from a cement matrix [23].

Table 4
Stiffness and crack spacing parameters obtained from the experimental data and used in the theoretical model

Mix	Designation	Stiffness			Crack spacing			
		$X_1 + X_2$*exp($-X_3$*ε_i)			$S_1 + S_0$*exp($-\alpha$*($\varepsilon_i - \varepsilon_{mu}$))			
		X_1	X_2	X_3	S_1	S_0	α	ε_{mu}
A	ARGNP	309.1	1921	319	$-1.16E+1$	$3.65E+01$	$5.59E+01$	$-8.71E-4$
B	ARG-FA	394.4	2429	586	$3.93E+1$	$9.54E+0$	$1.53E+2$	$7.51E-3$
C	ARG-P900	501.4	3154	439	$8.74E+0$	$4.85E+2$	$1.90E+2$	$-1.08E-2$
D	PE-P900	54.1	2260	319	$3.92E+1$	$6.97E+0$	$1.76E+2$	$7.64E-3$
E	PP-P900	329.2	7679	471	$4.82E+0$	$4.89E+2$	$1.64E+2$	$-1.26E-2$

4. Lamina stresses and deformations prior to distributed cracking

A general 2D plane stress approach for the treatment of cross ply laminate composites made with various fiber and matrix materials has been proposed earlier [10]. In the present approach a 1-D treatment of the model is presented while the procedure can be easily extended to other cases such as biaxial and flexural modes. The cross-section of the specimen throughout its depth is divided into several layers referred to as lamina and the stresses and strain within each lamina are assumed to remain uniform. Each lamina is modeled as an orthotropic sheet in plane stress with directions "1" and "2" representing the longitudinal and transverse direction of yarns as shown in Fig. 2. θ is an angle measured from the axis of loading to the longitudinal direction of yarn "1", for all tests presented here are concentric loading ($\theta = 0$). Parameters h_k and h_{k+1} refer to the coordinates at the top and bottom of lamina number "k" in a stack of "n" laminates. The property of a layer is specified using the material properties and volume fraction of components. The formulation is applicable to uniform or linear strain field. An incremental approach is used to impose a constant tensile strain field across the cross-section for a uniaxial tension case. At each iteration level the strains at the top and bottom of each lamina are updated and applied to the orthotropic model to compute ply stress and identify the state of cracking [15]. The equivalent elastic stiffness assumes the fabric remains elastic and sums their contributions from each layer to the overall value. The model proposed for the stress–strain response of the matrix, fabric, and the composite is shown in Fig. 3. Four distinct zones are identified using roman numerals with two zones prior to BOP and two zones after the BOP range.

Zone I corresponds to the elastic-linear range where both matrix and the fabric behave linearly. This zone is modeled using composite laminate theory with an iso-strain model to relate the properties of fabric and matrix to the composite response, i.e. employing rule of mixtures for longitudinal modulus. Due to low volume fraction of fibers (normally less than 10%) the stiffness of the lamina is dominated by matrix properties. This zone is terminated by initial crack formation in the matrix phase at a point labeled "A" and designated as σ_{t1} at the strain level ε_{t1} [16] (reported as of σ^{-}_{BOP} from

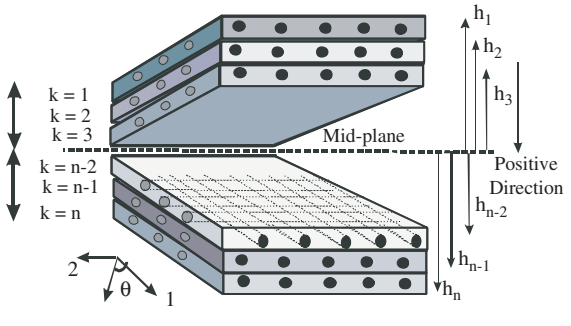

'1' Longitudinal Yarn Direction
'2' Transverse Yarn Direction
Θ Angle between the longitudinal direction and axis of loading (Uniaxial tension, θ=0)

Fig. 2. Definition of lamina and coordinates used in generating stiffness coefficients.

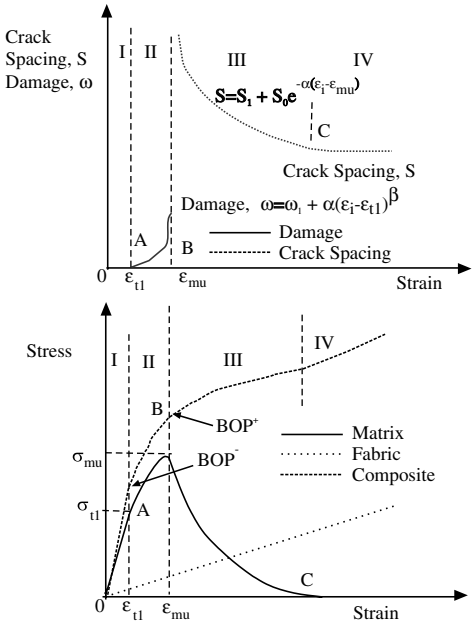

Fig. 3. Crack spacing, damage evolution, and stress–strain response for matrix and the composite.

experiments). After the initiation of cracks in the matrix, its load carrying capacity does not vanish as the cracks are bridged by the longitudinal yarns.

The second range (Zone II) is defined as between the two stress levels of σ^{-}_{BOP} and σ^{+}_{BOP}. During this stage, matrix cracks begin to form and propagate across the width of the specimen, however, no single crack has traversed the entire length of the specimen. This range (Zone II) defines the formation of first complete crack across the cross-section between points "A" and "B". The crack is modeled as a dilute concentration of cracks in a medium, and the stiffness degradation is assumed to follow a self consistent approach and degrade up to the BOP^{+} level according to a single scalar damage parameter 'ω'. The form of the evolution of the damage parameter proposed by Karihaloo [17] is expressed as a power law:

$$\omega(\varepsilon_i) = \omega_1 + \alpha(\varepsilon_i - \varepsilon_{t1})^{\beta} \quad \varepsilon_{t1} < \varepsilon_i < \varepsilon_{mu} \tag{2}$$

where ε_i is strain at which the damage parameter is computed; ε_{t1} is strain at first crack; ω_1, α, and β are constant terms in the power law model. The values of these constants are of (taken from Ref. [14]) $\alpha = 1.0$, $\beta = 0.3$, and $\omega_1 = \varepsilon_{t1}H$ where H is the gage length of the specimen used. Parameter σ_{t1} is the tensile strength of the matrix paste without the presence of fibers, and $\varepsilon_{t1} = \sigma_{t1}/E_{m0}$ was defined as the strain at failure under uniaxial tension for the paste in an unreinforced condition as shown in Fig. 3. The gradual decrease in the stiffness of the matrix starts at the plain matrix strength of σ_{t1}. A damage model by Horii [18] and Nemat Nasser and Hori [19] was used to simulate the decrease in the stiffness in the cracked matrix as the strain increases. Stiffness parameter $E_m(\omega)$, as a function of damage and initial matrix elastic modulus E_{m0} in Zone II was defined:

$$E_m(\omega) = \frac{E_{m0}}{1 + \frac{16}{3}\omega(1 - \nu_m^2)} \tag{3}$$

where ν_m is the Poisson ratio of the matrix. This value of matrix stiffness is used in the rule of mixtures to obtain the longitudinal stiffness of the lamina E_1 (ω). A modified rule of mixture is used in modeling the stiffness computation of a lamina according to Eq. (4):

$$E_1(\omega) = E_f V_f + E_m(\omega)(1 - V_f) \tag{4}$$

where E_f is the stiffness of the fiber; V_f is the volume fraction of the fiber. The stress is computed using an incremental approach by adding the products of strain increments by the effective stiffness at that level. The stress in the matrix phase beyond the elastic range is calculated incrementally as

$$\sigma_1^i(\omega) = \sigma^{i-1} + \Delta\sigma_t^i = \sigma_{t1} + \sum_{n=1}^{i} E_m(\omega)(\varepsilon_n - \varepsilon_{n-1}) < \sigma_{mu} \quad \varepsilon_{t1} < \varepsilon_i < \varepsilon_{mu} \tag{5}$$

The max stress in the matrix phase is achieved at a strain level of ε_{mu} described in the next section using Eq. (5) and is referred to as σ_{mu}.

The post BOP stage is characterized by formation of distributed cracking in Zone III, and its initiation is represented by parameters S_0, S_1, α, and ε_{mu} (Eq. (1)). The stiffness of the fabric cement system is sufficiently high to keep the newly formed cracks from widening and thus promoting additional cracking. This stiffness affects the rate of reduction of crack spacing, or α parameter.

Zone IV is dominated by progressive damage and characterized by a crack widening stage ultimately leading to failure by fabric delamination, failure, or delamination. This zone is asymptotically terminated at the saturation crack spacing represented by parameter S_1. The behavior of both the matrix and the fabric in addition to their interaction is studied in each of these four ranges, and the formulations are compiled together to present a comprehensive material simulation model.

5. Lamina stresses and deformations in the distributed cracking zone

Zone II terminates at a damage level corresponding to the stress at the BOP (σ^{+}_{BOP}) level which is also ultimate strength of matrix in the presence of fibers σ_{mu}. The degraded stiffness at each strain value from ε_{t1} up to the BOP strain level (ε_{mu}) is computed and used to calculate the stress. The parameter ε_{mu} may theoretically be obtained using the ACK approach [20] or other methods [21] which predict the strain capacity of the matrix phase in the presence of fibers as shown in Eq. (6).

$$\varepsilon_{mu} = \left[\frac{12\tau\gamma_m E_f V_f^2}{E_c E_m^2 r V_m}\right]^{\frac{1}{3}} \tag{6}$$

where τ is the shear strength of the matrix; γ_m is the fracture toughness of the matrix; E_c is the composite modulus; r is the fiber radius and V_m is the volume fraction of the matrix. This equation has been verified to be applicable for the cement based materials by showing that the strength of the matrix is increased in the presence of fibers [22]. The experimentally obtained values for ε_{mu} correspond to the values reported as $\varepsilon_{BOP(+)}$ as reported in Table 3. Depending on the fabric cement system used, in the current study, γ_m/r in the range 0.5–5.0 N mm/mm resulted in a good correlation between experimental and simulations of the stress and strain at BOP level.

Beyond the BOP level, Zone III is dominated by formation of parallel microcracking. The gradual reduction of matrix stress levels in the vicinity of the cracked matrix is referred to as the softening zone. In this zone the matrix cracks widen and while there may be no

localization in the strain softening zone, the response is modeled by contributions from a softening matrix and the fabric pullout force. The stress–strain response of matrix in the post peak region is assumed to be an exponentially decaying function of the maximum stress and asymptotically approach zero.

$$\sigma_1^i(\varepsilon_i) = \sigma_{mu} e^{-q(\varepsilon_i - \varepsilon_{mu})} \quad \varepsilon_i > \varepsilon_{mu} \tag{7}$$

where q represents the exponent coefficient affecting the rate of decay in stress from the peak composite stress. Typical value of q between 0.1 and 5.0 gives a reasonable rate of stress drop in the post peak region of the matrix phase. The definition of strain in this region is gage length dependent and the present approach uses the mean strain over the length of several cracks in the matrix. As the specimen undergoes strain softening, an exponential decaying stiffness similar to Eq. (7) utilizing the stiffness at peak was used. The modulus $E_m(\varepsilon_i)$, computed for each strain level ε_i, was proportional to the reduction of the stress from the peak value.

6. Theoretical simulation of fabric pullout

In the Zone III of loading, the cross-sections containing matrix cracks are held in equilibrium due to the fabrics which carry the load by bond and eventually fabric pullout mechanism. As fabrics bridge across an existing matrix crack, the stress is transferred back into the matrix through the interfacial zone. The magnitude of the shear stress is a function of the contact bond stiffness and the frictional properties between the two surfaces. Conceptually, the higher the bond, the higher tensile load can be resisted. Both experimental and theoretical values for the contact bond stiffness of a fabric under pullout conditions were used. The experimental stiffness values, K, were obtained from fabric pullout tests conducted by Sueki [13,23]. These parameters are reported in Table 3 for the various fabric–matrix combinations of mixtures A–E. The experimental values can be used as a constant linear elastic spring, k across the cracked matrix. The theoretical method to obtain the entire debonding and pullout–slip model is presented in Appendix I. This approach models two mechanisms that are responsible for the overall stiffness of a fabric. In addition to the bond stiffness of a longitudinal yarn, additional stiffness is provided due to the anchorage at the junction point of two yarns. This junction point serves to transfer load to the transverse yarns, which by deforming, tend to transfer load away from the longitudinal yarns. A beam on elastic foundation formulation was introduced to model this response and obtain the stiffness parameters of a junction as described in Appendix I. Using the bending mechanism of the transverse yarns, the stiffness of a junction was used to compute the compliance of a fabric under pullout condition. This compliance was utilized in calculation of average strain once distributed cracking was the dominant mode (Zones III and IV). The nonlinear model is capable of predicting the initial linear loading, partial debonding, and fabric pullout, and compared to a constant stiffness approach which assumes a linear spring model across the crack.

7. Computation of the compliance of cracked composite

The displacement of the specimen is obtained by integrating the strain components in the uncracked segments and adding it to the slip parameters obtained from the cracked regions. The crack spacing function defined in Eq. (1) and its parameter in Table 4 determine the mean crack spacing for calculations of displacements. A representative volume element of the sample in Fig. I.1 shows a single crack across a representative specimen with length equal to average crack spacing. The slip for a given load is adjusted for a factor of 2 to represent crack opening across two faces of a crack. The total displacement of the sample is the combination of the slip and the elongation obtained through the uncracked segments of the specimen, which were assumed to carry an average strain of ε_{mu} defined theoretically according to Eq. (6). Subsequent loadings of a cracked layer results in a change in the magnitude of the crack spacing as obtained from the damage evolution law. The response of a matrix in the strain-softening zone asymptotically approached to a level of zero stress. Function $C(P)$ represents the compliance of the debonded fabric as a function of applied load and is obtained from the pullout load–slip response defined using Eqs. (I.1) and (I.2) (from Appendix I)

$$C(P) = \frac{U(L)}{P} = \frac{\frac{-2\pi r\tau_{max}}{\beta_2 \coth(\beta_2(L-L_d))} + \tau_f(2\pi r)L_d + \sum_{i=1}^{n} K_b u(x_i)}{\frac{P-\tau_f L_d}{E_f \pi r^2 \beta_2}\coth(\beta_2(L-L_d)) + \frac{P-\frac{1}{2}\tau_f L_d}{E_f \pi r^2} L_d} \tag{8}$$

where $U(L)$ is the slip for embedded length L; P is the pullout load; τ_{max} and τ_f are the maximum and residual shear strength of the interface; r is the fiber radius, L_d is the debonded length; K_b is the equivalent spring stiffness obtained from beam on elastic foundation system; $u(x_i)$ is the deformation in direction of the pullout load; parameter $\beta_2 = \sqrt{\frac{G_i}{E_f \pi r^2}}$, where G_i is the shear modulus of the interface. The average displacement $\Delta(\varepsilon_i)$ of the specimen is expressed by

$$\Delta(\varepsilon_i) = \bar{\varepsilon} H = \left[\varepsilon_{mu} + 2P(\varepsilon_i)\frac{1}{S(\varepsilon_i)}C(P)\right]H \quad \varepsilon_i > \varepsilon_{mu} \tag{9}$$

where H is the gage length. This approach states that the average strain is primarily related to the magnitude of

crack spacing, the force applied, and the stiffness (or compliance) of the bond between the fabrics and the cement matrix. Using the updated crack spacing, the quasi-elastic stiffness parameters are obtained and used to calculate the stress and load for that increment. One way to simplify this approach is to assume a linear approach by using constant bond stiffness throughout the test. This constant bond stiffness has been calculated using the experimental pullout–slip response and is defined as K reported in the last column of Table 3. Simplification of Eq. (9) to a constant stiffness measure would require assumption of zero debonded length (i.e. $L_d = 0$) resulting in the following:

$$\Delta(\varepsilon_i) = \bar{\varepsilon}H = \left[\varepsilon_{mu} + 2P(\varepsilon_i)\frac{1}{KS(\varepsilon_i)}\right]H \quad \varepsilon_i > \varepsilon_{mu} \tag{10}$$

8. Formulation for a laminate in tension

Depending on the state of normal strain in each lamina, the stiffness is calculated incrementally and applied to the orthotropic model to calculate lamina stress. Due to the incremental nature of the solution, load redistributions were not considered. The constitutive relations for a general orthotropic material include the stiffness matrix which relates the stress and strain within a lamina loaded in its principal directions. The stiffness of the matrix phase due to cracking is updated with each increment of applied strain. An elastically equivalent compliance matrix is calculated with the updated elastic properties.

$$\begin{aligned} \Delta\sigma^i &= E_1(\omega)\Delta\varepsilon^i \\ \sigma^i &= \Delta\sigma^i + \sigma^{i-1} = E_1(\omega)\Delta\varepsilon^i + \sigma^{i-1} \end{aligned} \tag{11}$$

The average stiffness parameter for the lamina is obtained as $\bar{A}$ which relates the strains into average normal stress for the laminate loaded in the principal material direction [24].

$$\bar{A} = \sum_{m=1}^{n} E_1(\omega)(h_m - h_{m-1}) \tag{12}$$

$\bar{A}$ is the extensional stiffness of the material, it is used to compute P the force per unit length of cross-section and takes into account the layers which have cracked, softened, or fractured. With knowledge of incremental strain the lamina stress is computed for each loading step and the results are added to the loads and strains from previous iteration, i.e. the applied load at the step ith (P_i) was represented as

$$P_i = P_{i-1} + \Delta P_i = P_{i-1} + \bar{A}\Delta\varepsilon_i \tag{13}$$

The algorithm for calculation of load-deformation in the axial response is as follows: the geometrical dimensions of the lamina and the stacking sequence are defined. The strain distribution is imposed incrementally, and the stiffness coefficients of $\bar{A}$, are calculated and used to obtain the stress. If the stresses meet the failure criterion, the stress and stiffness are adjusted according to the constitutive response and the material properties are updated for subsequent analysis. The ultimate strength of fabric material F_{fu}, was used as the point of termination of computation and used to define the failure of composite at a stress defined as σ_{cu}. These values were obtained by multiplying the number of yarns per unit thickness (n/t) by the experimentally obtained strength of plain fabrics

$$\sigma_{cu} = V_f\sigma_{fu} = nF_{fu}/t \tag{14}$$

The ultimate strength F_{fu}, is dependant on the fabric type and geometry, furthermore, experimental observations indicated that in majority of cases, the ultimate failure was due to fabric–paste bond, the strength of the lamina was not significant in comparison with the degradation of the stiffness and the overall stress–strain response.

In order to calibrate the empirical parameters introduced, an approach was used to fit the proposed models to the relationship between the crack spacing and the stiffness degradation according to Eqs. (1)–(3), (6) and (7). A comparative response function is shown for two fabric systems according to Fig. 4. In this plot experimental data for crack spacing and tangent stiffness are plotted at various strain levels for two fabric systems, low modulus PE fabric and high modulus AR-Glass fabric. The experimental values are shown as the solid markers and the theoretical simulations based on the empirical models of Eqs. (2)–(7) are shown as lines through the experimental data. It is noted that although these formulations are all based on the applied strain, and even though the strain as the independent variable is eliminated in this figure, still a good correlation between these independent measurements of damage

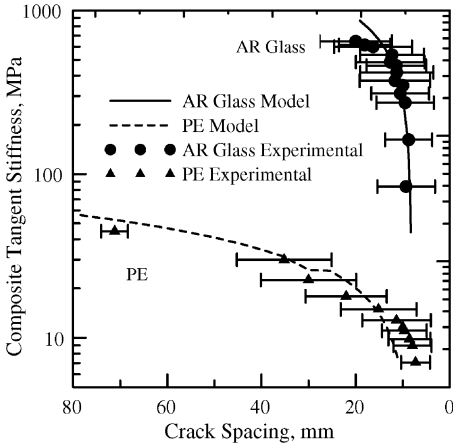

Fig. 4. Comparison of two fabric systems in stiffness degradation as a function of crack spacing.

are obtained. It is furthermore shown that the stiffness degradation in AR-Glass fabric decreases by about an order of magnitude over a small range of crack distribution. The stiffness degradation in PE system is also distributed over an order of magnitude range, but compared to AR-Glass fabrics is operational at an entirely different crack spacing range. The range of cracking in PE systems is much longer as compared to the AR-Glass fabric systems.

9. Analysis of the results

A summary of a parametric study is presented to examine the sensitivity of the model to a range of parameters including volume fraction, stiffness of fabric, interface bond strength, and matrix properties is presented. A more comprehensive discussion is available elsewhere [25]. There are three potential ways to increase the post cracking stiffness of the composite; increasing the volume fraction of fabric material, increasing the stiffness of the fabric material, or enhancing the bond between the fabric and matrix. These three aspects point out that as the fabric volume fraction increases, the stiffness of the composite in the post cracking range increases by two different mechanisms, increasing the BOP level (as shown in Eq. (6) ACK Model) in addition to the post crack stiffness due to the number of fabric layers intersecting each crack. The latter is more dominant since the relationship is linear while the former mechanism is dependant of cubic root of the volume fraction.

The effect of stiffness of the fabric on the overall stress–strain response of the composite also shows that as we cover the low to high modulus fabrics used, representing, AR-Glass, PP, and PE, a change of stiffness in the post BOP range is by an order of magnitude [25]. Increasing the stiffness of the fabric material has a direct effect on the overall stiffness characteristics of the system, while increasing the bond decreases the load transfer length back into the matrix. Therefore a direct correlation exists between the stiffness of the fabric and reduction in crack spacing, which will be studied during the comparison with experimental data.

The significance of the effect of stiffness of the interface on the stress–strain response of the composite has been shown in a parametric study [25]. When the bond is weak, pullout of the fabric takes place at the expense of additional cracking. Fig. 5a and b study the effect of bond strength of the fabric material on the fabric pullout and the tensile stress–strain response of composites. First the fiber pullout model is represented with two different shear strength levels of 2.13 and 2.91 MPa. These curves are compared with the experimental pullout–slip response of PP fabrics. Note that increasing the bond strength, increases the load carrying capacity at any slip

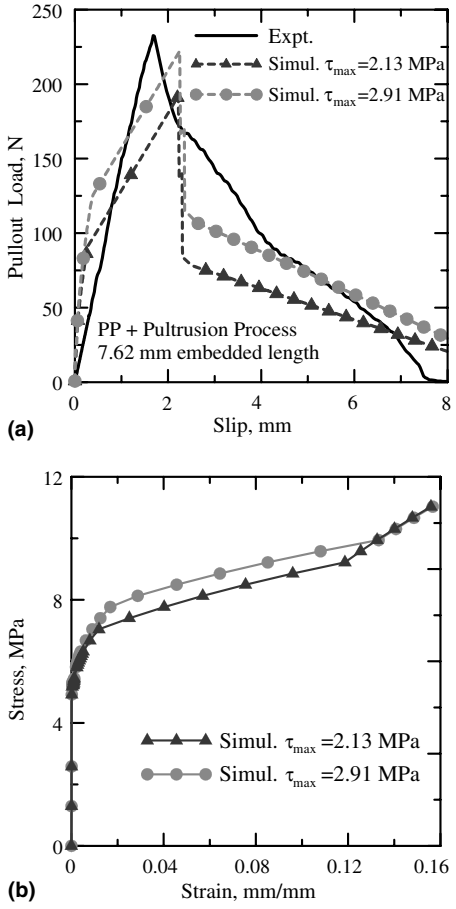

Fig. 5. Behavior of the model with varying values of bond strength of the PP fabric. (a) Pullout test results and model simulation for two different shear strength values. (b) Simulation of tension test.

level and the ultimate pullout force. These curves are used as the nonlinear stiffness models for the cracked matrix. The model uses constant crack spacing evolution terms (S_0, S_1, α, and ε_{mu}) in both cases, hence it is not possible how the mode of failure changes from distributed cracking at high bond strength to crack widening at low bond strength. The simulation of stress–strain diagram for the composite is shown in Fig. 5b. Note that lower shear strength values result in a lower load carrying capacity. In order to make this simulation possible, only the interface shear strength (τ_{max}) of the composites were altered from 2.13 to 2.91 MPa, and the resulting pullout response according to Eq. (I.1) was used in the analysis of the tensile test data. After the matrix cracking is completed, the load is primarily carried by the fibers, hence the two curves converge.

9.1. Comparison with experimental results

The parameters used in the analytical model were calibrated with the experimental results of stress–strain and crack spacing versus strain response of several composite systems. Several case studies were used: three fabric

types AR-Glass, PE and PP, two matrix formulations, with and without addition of fly ash, and two processing parameters, with low and high pressures applied on top of the composite at its fresh stage. Tables 3 and 4 present the summary of mechanical stress–strain, stiffness degradation and crack spacing parameters of these specimens.

The first case study evaluated the effect of pressure applied during preparation of the specimens. To study this variable, two different pressure levels of 1.7 kPa (Series A) and 15 kPa (Series C) were applied on top of the laminates which affected the penetration of matrix in between fabric openings and the quality of interface bond. Fig. 6 presents the experimental and simulated effect of the applied pressure on the stress–strain and crack density. The model can successfully predict the tensile responses based on the crack spacing distributions for both cases of pressures. The initial cracking stress, the post crack stiffness, the ultimate strength, and also the mean crack density are all dependant on the level of applied pressure. An increase in the pressure increases the tensile strength of the composite by about 83%, and the saturation crack density decreases from 18 mm to 9 mm suggesting better bonding under high pressure. Moreover, Fig. 6 also shows that crack widening is the control mechanism of the low-pressure composites, as the crack spacing function beyond strain of 2% is not significantly changed. This value of strain is significantly less than the strains (3%) obtained for the high-pressed composites. The above discussion suggests relatively poor bond of the low-pressed system which can be effectively modeled using the interface parameters chosen. On the other hand, enhanced interaction between the fabric and the cement matrix is indicated for the high-pressed composite as most of the tensile response is controlled by multiple cracking mechanisms due to stress transfer between the fabric and the matrix. One can clearly see the effect of the pressure applied after the pultrusion process on the model predictions of tangent stiffness of the composite. This change is integrated in the model by means of the crack spacing parameters used (Fig. 6 and Table 4). Low pressure results in low stiffness, whereas the composite with the high pressure is much stiffer through the whole range of loading.

The second study is to evaluate the effect of flyash on the composite. The performance of plain portland cement composite (Series A) was compared to another mixture (Series B) where 40% by volume of the portland cement was replaced with Class F flyash. Both systems use AR Glass fabrics. Using parameters in Table 4 results in the simulation shown in Fig. 7. Note that the matrix modification by the use of flyash affects the overall response of the system and the crack spacing parameters, resulting in much higher post crack stiffness as compared to the control sample. Use of flyash improves the bond strength and anchorage of the fabric and thus the cracking stage is a more dominant mechanism as compared to crack widening. The crack saturation density in the control specimens does not decrease below 20 mm as compared to 12 mm for the flyash modified mixtures. In order to simulate these experimental observations, a bond strength of 2.62 MPa was used for the matrix with 40% flyash as compared to a bond strength of 1.76 MPa used for the control sample. These bond values resulted in different fabric pullout–slip responses, directly affecting the tensile response.

The effect of flyash particles on stiffening the specimen can be shown in the microstructural examination of fabric cement composite systems. Due to their size

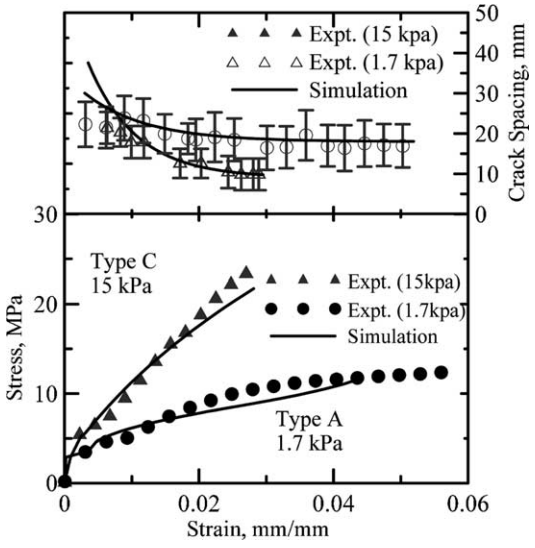

Fig. 6. Stress and crack spacing versus strain for samples with AR-Glass fabric (with low pressure, 1.7 kPa Series A, and high pressure 15 kPa, Series C) compared with the theoretical model.

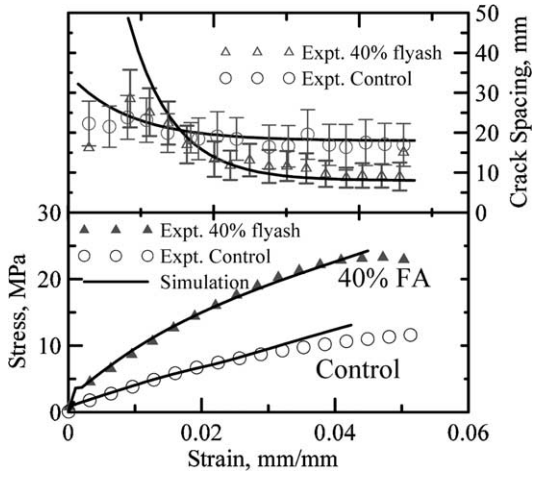

Fig. 7. Crack spacing and stress versus strain for samples with AR-Glass fabric (with flyash Series B, and without flyash Series C) as compared with the theoretical model.

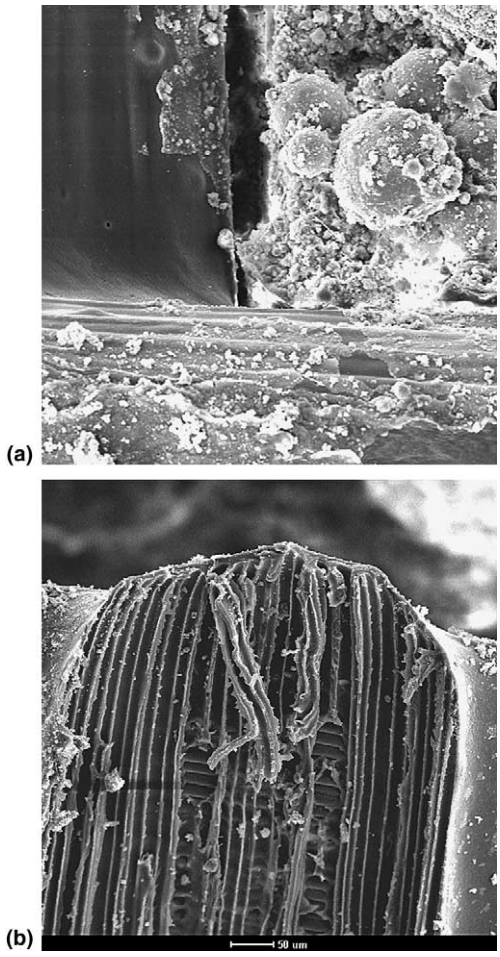

Fig. 8. (a) SEM image of sample with AR-Glass and 40% flyash showing the flyash particles filling the region close to the bonded junction. (b) Failure of the bonded junction revealing the strength of the coated component as a weak point in the failure of the longitudinal versus transverse yarn.

and shape, flyash particles can easily occupy the voids at the junction of the yarns in the fabric. Fig. 8a shows a group of flyash particles located at the fabric joint resulting in densification of the interface layer and thus improvements in anchorage of the fabrics. Fig. 8b shows the failure of a junction bond in the AR-Glass fabrics which is a direct consequence of proper anchorage of the transverse yarns of the fabric. Note that the fracture of a single junction contributes to the sequential debonding of the yarns, and extends the load carrying capacity of the fabric and toughening the composite mechanisms. Modeling of the sequential failure of the fabric response is addressed in Appendix I.

The third study was carried out with low modulus PE fabric cement composites, labeled as "D" type in Tables 1–3. Fig. 9 shows two replicate samples of PE cement composites along with the model response. Note that both the stress–strain and the crack spacing response of both samples are sufficiently well simulated with the theoretical simulations. While the saturation crack spacing of these specimens are much smaller than glass fabric specimens, the post cracking stiffness values are lower due to the lower stiffness of the polymeric fibers used. The general agreement of both the crack spacing and stress versus strain responses clearly show that the proposed methodology is applicable to a range of composites. In this simulation the nonlinear approach for the fabric pullout model described in Appendix I was used. Initial stiffness of the composite as obtained in the experimental results and reported in Table 3 equal to 1.9 GPa was used. This value is much lower than the expected value of about 15–20 GPa for cement based materials.

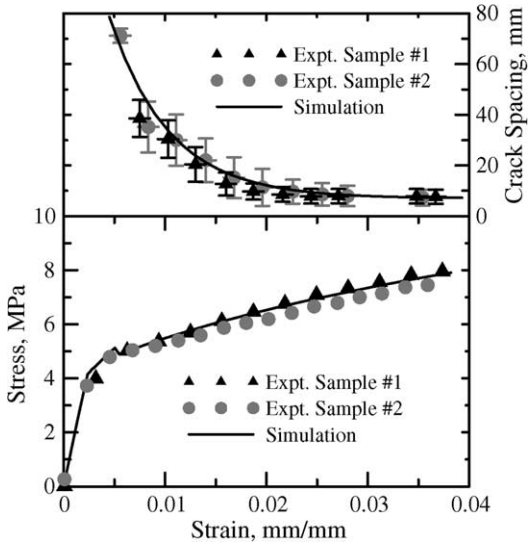

Fig. 9. Stress and crack spacing plots plotted versus strain for two samples with polyethylene (PE) fabric along with the theoretical model response which gives the fit for the crack spacing and the stress–strain response.

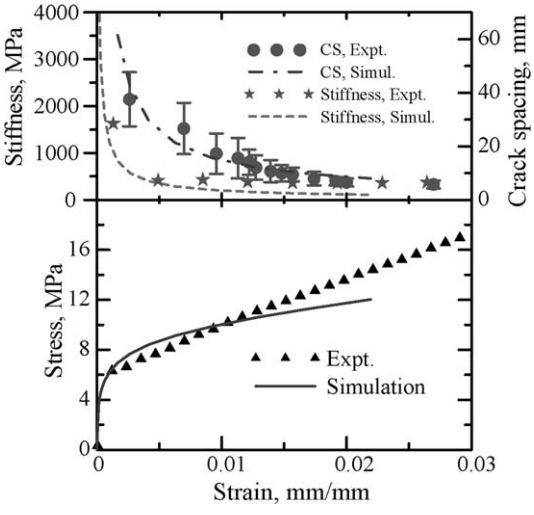

Fig. 10. Crack spacing, stiffness, and stress plotted versus strain for a sample with PP fabric compared with the theoretical model response.

The final study investigates the using of simple linear bridging models to simulate the experimental results. In order to compare the present model using the simplifications for the bridging mechanism, a constant bridging stiffness of $k = 109$ N/mm for PP samples (labeled "E") was used in lieu of the nonlinear response. The simulation of stiffness degradation and crack spacing formation along with the stress strain responses are shown in Fig. 10. Note that the linear pullout response can model the transition of the load response, crack spacing and also the stiffness degradation as a function of strain. The post BOP stress–strain response is underestimated by using the simplified linear stiffness model, and higher stiffness of the fabric layer is required to better simulate the full stress–strain response.

10. Conclusions

A procedure is presented to relate the properties of the matrix, fabric, interface and the damage parameters to the overall mechanical response of fabric reinforced cement based composites. The crack evolution and stiffness degradation can be related to the applied strain, and used in an incremental approach with composite laminate theory to simulate the uniaxial tensile response of the composites. The pullout data of the fabrics was used in both a linear and nonlinear approach to simulate the crack bridging force across the matrix cracks. The model simulation data is compared with wide range of experimental tests. A good fit is obtained between the calculated and the experimental values for various matrix formulations, fabric types, and processing parameters. Experimental observations can be explained by the simulation methodology using material parameters.

Acknowledgements

The authors acknowledge the support from National Science Foundation, program 0324669-03, and the BSF (United States Israel Binational Science Foundation) program 84380101.

Appendix I

A theoretical basis has been proposed to analyze the experimental results of fabric pullout from a cementitious matrix. The load transfer across a matrix crack can be calculated using a closed form fabric cement bond model [26]. A model for pullout of straight yarns based on shear lag approach is used as the basis and the debonding and pullout using frictional and adhesion bond is modeled. The effect of transverse yarns in woven and bonded fabrics are handled using a periodic arrangement of linear springs providing anchorage at the warp/fill junctions (warp and fill are the yarns parallel and perpendicular to load direction, respectively). Anchorage at the point of intersection of yarns is attributed to the connection of the warp and fills yarns and the restraint offered by the fill yarns in redistributing the load. Anchorage may also be caused by the surface curvature of the yarn in a woven fabric. The simulation results have been compared with the experimental results of three fabric types and three different sample making procedures [12]. The model predictions verified the experimental results quite well.

A segment of matrix between two bridged cracks is used. The length is specified as the average crack spacing $S(\varepsilon)$, which is a function of the applied global strain. The crack is placed in the middle of this specimen. A uniformly loaded uniaxial tensile stress is applied at the ends of the sample. This stress is transferred to the fabric and then back into the matrix over the specimen length. A portion of the stress passes through the traction of the crack and another portion through the fabric across the crack. The stress transfer across the strain softening matrix is handled by means of exponential decay formulation of Eq. (7). According to the model for Fabric pullout, as shown in Fig. I.1 load on the fabric can be divided in three portions: load carried by the debonded region, P_d, load carried by the bonded region, P_y, and load transferred at the junctions points to the transverse yarns P_b. In the debonded region two parameters are important, the debonded length, L_d, and the constant frictional shear stress acting along this length τ_f [27]. In the bonded region, a shear lag mechanism is operating with a decaying shear stress due to parameter β_2 which models the stiffness of the interface. This theoretical procedure was used in order to characterize the pullout–slip response of a fabric according to the de-bonded length, and the number of active junctions in redistributing the load. The general load–slip relationship for a debonding fabric is expressed as

$$P = P_d + P_y + P_b = \tau_f(2\pi r)L_d + \frac{-2\pi r\tau_{max}}{\beta_2 \coth(\beta_2(L - L_d))} + \sum_{i=1}^{n} K_b u(x_i) \quad \text{(I.1)}$$

$$U(L) = \frac{P - \tau_f L_d}{E_f \pi r^2 \beta_2} \coth(\beta_2(L - L_d)) + \frac{P - \frac{1}{2}\tau_f L_d}{E_f \pi r^2} L_d \quad \text{(I.2)}$$

where $K_b = \frac{2k}{\lambda} \frac{\sinh(\lambda l) + \sin(\lambda l)}{\cosh(\lambda l) + \cos(\lambda l) - 2}$

$$\beta_2 = \sqrt{\frac{G_i}{E_f \pi r^2}} \qquad \lambda = \sqrt[4]{\frac{k}{4EI}} \quad \text{(I.3)}$$

In these equations, $k = bk_0$. k_0 is the modulus of foundation in N/m^3, b is the constant width of the beam in

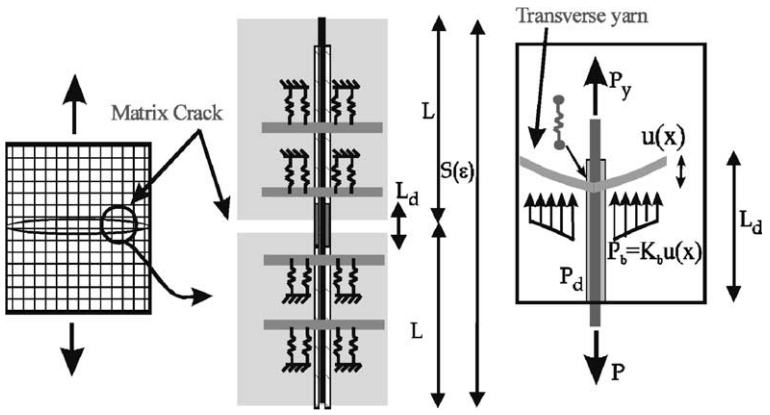

Fig. I.1. Schematic of the distributed cracking and the debonding model: (a) composite segment with the length of average crack spacing; (b) beam on elastic foundation model; (c) load contributions by the debonded region P_d, bonded region P_y, and junction P_b.

Table I.1
Values of parameters used in fabric pullout model [23]

Fabric material	Nominal E for matrix (MPa)	Nominal E for fiber (MPa)	Nominal E for beam (MPa)	Nominal E for foundation (N/m^3)	Strength for anchorage (N)
AR-Glass	4000	3144	2000	4000	8
PE		176	0.1		1
PP		1380	3.5		4

contact with the foundation and EI is the flexural rigidity of the yarn treated as a beam. In the present approach, b is considered as thickness of yarn and I is calculated from fill-yarn geometry [28]. k_0 and E are considered as the values related to matrix and fiber interface. Table I.1 presents the parameters used in the generation of the pullout–slip response of different fabric systems. Fig. I.2 presents a simulation of the fabric pullout force–slip relationship experiments for two fabrics studied: AR-Glass and PE. Note that the initial response of the two curves up to the peak point is well modeled using the present approach. The sudden drop in the load response corresponds to the failure of the junction points at each increment of the connection between the warp and fill yarns, or the junctions in the cross yarn attachments.

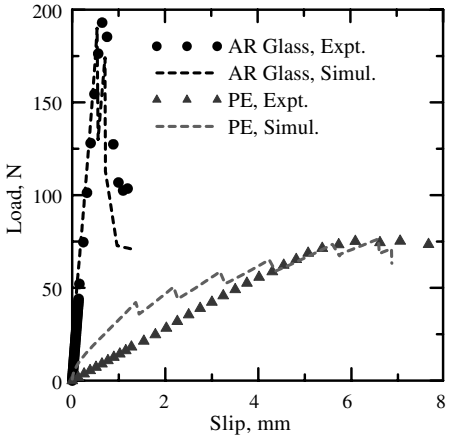

Fig. I.2. The pullout response of the nonlinear fabric debonding model.

References

[1] Brameshuber W, Koster M, Hegger J, Voss S, Gries, T, Barle M, et al. Textile reinforced concrete (TRC) for integrated formworks. In: 12. internationale techtextil-symposium für technische textilien, vliesstoffe und textilarmierte werkstoffe. Messe Frankfurt GmbH, Frankfurt; 2003. 4.23.-CD-Rom.

[2] Kruger M, Ozbolt J, Reinhardt HW. A new 3D discrete bond model to study the influence of bond on structural performance of thin reinforced and prestressed concrete plates. In: Naaman AE, Reindhart HW, editors. Proceedings of the fourth international RILEM workshop on high performance fiber reinforced cement composites (HPFRCC4). Ann Arbor; 2003. p. 49–63.

[3] Meyer C, Vilkner G. Glass concrete thin sheets prestressed with aramid fiber mesh. In: Naaman AE, Reindhart HW, editors. Proceedings of the fourth international RILEM workshop on high performance fiber reinforced cement composites (HPFRCC4). Ann Arbor; 2003. p. 325–36.

[4] Brameshuber W, Brockmann T, Hegger J, Molter M. Textilbeton-Betontechnologie und Tragverhalten. Untersuchungen zum Textilbewehrten Beton, Beton 09/2002, Seiten; 2002. p. 424–9.

[5] Jesse F, Curbach M. A new approach for determining geometrical properties of glass fibre reinforcement in GRC composites. In: di Prisco M, Felicetti R, Plizzari GA (Hrsg.), Fibre-reinforced concretes: Proceedings of the sixth international RILEM-symposium—BEFIB 2004. Varenna, Bagneux: RILEM; 2004. S. 267–78.

[6] Peled A, Mobasher B. Pultruded fabric–cement composites. ACI Mater J 2005;102(1):15–23.

[7] Reinhardt H-W, Krüger M, Grosse CU. Concrete prestressed with textile fabric. J Adv Concrete Technol 2003;1(3):231–9.

[8] Talreja R. Stiffness properties of composite laminates with matrix cracking and interior delamination. Eng Fract Mech 1986;25(5/6): 751–62.
[9] Mobasher B, Stang H, Shah SP. Microcracking in fiber reinforced concrete. J Cem Concr Res 1990;20:665–76.
[10] Mobasher B. Micromechanical modeling of filament wound cement-based composites. ASCE J Eng Mech 2003;129(4):373–82.
[11] Häußler-Combe U, Jesse F, Curbach M. Textile reinforced concrete-overview, experimental and theoretical investigations. In: Li VC et al., editors. Fracture mechanics of concrete structures. Proceedings of the fifth international conference on fracture mechanics of concrete and concrete structures, Ia-FraMCos, Vail, CO, USA, vol. 204, 12–16 April 2004. p. 749–56.
[12] Sueki S. An analytical and experimental study of fabric-reinforced, cement-based laminated composites. Thesis (MS), Arizona State University, 2003.
[13] Peled A, Mobasher B, Sueki S. Technology methods in textile cement-based composites concrete science and engineering. A tribute to Arnon Bentur. In: Kovler K, Marchand J, Mindess S, Weiss J, editors. RILEM Proceedings PRO 36; 2004. p. 187–202.
[14] Mobasher B, Peled A, Pahalijani J. Distributed cracking and stiffness degradation in fabric–cement composites. J Mater Struct, in press.
[15] Peled A, Mobasher B. Cement based pultruded composites with fabrics. In: Proceedings of the 7th international symposium on brittle matrix composites (BMC7). Warsaw, Poland; 2003. p. 505–14.
[16] Agarwal BD, Broutman LJ. Analysis and performance of fiber composites. 2nd ed. New York: John Wiley & Sons; 1990.
[17] Karihaloo, Bhushan L. Fracture mechanics and structural concrete. Harlow, Essex, England: Longman Scientific and Technical; 1995.
[18] Horii H, Hasegawa A, Nishino F. Process zone model and influencing factors in fracture of concrete. In G-28; 1987. p. 205–19.
[19] Nemat-Nasser S, Hori M. Micromechanics: overall properties of heterogeneous materials. 2nd ed. North-Holland: Amsterdam; 1999. 810 pp.
[20] Aveston J, Cooper GA, Kelly A. The properties of fiber composites. In: Conference proceedings National Physical Laboratory (IPC Science and Technology Press Ltd). Paper 1; 1971. p. 15.
[21] Mobasher B, Li CY. Effect of interfacial properties on the crack propagation in cementitious composites. J Adv Cem Based Mater 1996;4(3):93–106.
[22] Mobasher B, Shah SP. Interaction between fibers and the cement matrix in glass fiber reinforced concrete. American Concrete Institute, ACI SP-124; 1990. p. 137–56.
[23] Sueki S, Soranakom C, Mobasher B, Peled A. Pullout–slip response of fabrics embedded in a cement paste matrix. ASCE J Mater Eng, in review.
[24] Jones RM. Mechanics of composites materials. London: Taylor & Francis; 1998. 519 pp.
[25] Pahalijani J. An analytical and experimental study of fabric-reinforced. cement-based laminated composites. MS Thesis, Arizona State University, 2004.
[26] Peled A, Mobasher B, Sueki S. Technology methods in textile cement-based composites concrete science and engineering. A tribute to Arnon Bentur. In: Kovelr K, Marchand J, Mindess S, Weiss J, editors. RILEM proceedings PRO 36. March 2004. p. 187–202.
[27] Stang H, Shah SP. Failure of fiber-reinforced composites by pull-out fracture. J Mater Sci 1986;21:953–7.
[28] Hetényi M. Beams on elastic foundation. Ann Arbor: University of Michigan Press; 1946. 255 pp.